Inorganic Chemistry

pubs.acs.org/IC Article

# Amphiphilicity in Oxygen Atom Transfer Reactions of Oxobis(iminoxolene)osmium Complexes

Alexander N. Erickson, Jacqueline Gianino, Sean J. Markovitz, and Seth N. Brown*

Cite This: *Inorg. Chem.* 2021, 60, 4004–4014 Read Online

ACCESS | Metrics & More | Article Recommendations | Supporting Information

**ABSTRACT:** Oxobis(iminoxolene)osmium(VI) compounds ($^{R}$ap)$_2$OsO ($^{R}$ap = 2-(4-RC$_6$H$_4$N)-4,6-$^{t}$Bu$_2$C$_6$H$_2$O) are readily deoxygenated by phosphines and phosphites to give five-coordinate ($^{R}$ap)$_2$Os(PR′$_3$) or six-coordinate ($^{R}$ap)$_2$Os(PR′$_3$)$_2$. Structural data indicate that this net two-electron reduction is accompanied by apparent oxidation of the iminoxolene ligands due to their greater ability to engage in $\pi$ donation to the reduced deoxy form of the osmium complex. In ($^{R}$ap)$_2$Os(PR′$_3$)$_2$, the HOMO is a ligand-based combination of the iminoxolene redox-active orbitals, while the LUMO is a highly covalent metal-iminoxolene $\pi^*$ orbital. In the trans isomer, the HOMO is required to be ligand-localized by symmetry, while in the cis isomer, the ligands adopt a conformation that minimizes metal−ligand $\pi^*$ interactions in the HOMO. Kinetic studies indicate that the deoxygenations involve the rate-determining attack of the phosphorus(III) reagent on the five-coordinate oxo complexes. Varying the substituents of the aryl groups on the iminoxolene ligands or on the triarylphosphines has little effect on the rate of oxygen atom transfer, with the best correlation shown between oxygen atom transfer rates and the HOMO−LUMO gap of the oxo complexes. This suggests that the osmium oxo group shows a balance between electrophilic and nucleophilic character in its oxygen atom transfer reactions with phosphorus(III) reagents.

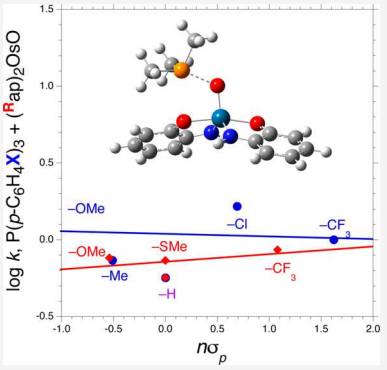


Downloaded via UNIV OF NOTRE DAME on March 15, 2021 at 18:36:18 (UTC).
See https://pubs.acs.org/sharingguidelines for options on how to legitimately share published articles.

## INTRODUCTION

Oxygen atom transfer (OAT) reactions are two-electron, inner-sphere redox reactions in which an oxygen atom is transferred from the oxidant to the reductant. Such reactions are typically slow between main group (phosphines, sulfides, and alkenes) substrates, but reactions between transition-metal oxo compounds and main group reductants are more rapid, leading to applications of transition-metal oxo compounds in catalysis.

The thermodynamic parameters of OAT reactions have been studied extensively,[1] revealing a large range of oxidizing power in OAT couples from the highly oxidizing (e.g., N$_2$O/N$_2$) to the highly reducing (e.g., R$_3$PO/R$_3$P). The mechanism of OAT reactions between metal oxo complexes and main group substrates has also been studied extensively, particularly the reactions of phosphines, which react cleanly with most metal oxo compounds to form phosphine oxides. Theoretical[2] and experimental[3] studies of this reaction paint a consistent picture wherein the phosphine attacks the oxo ligand directly to form an intermediate phosphine oxide adduct. An open coordination site at the metal center is not required, and indeed prior coordination of phosphine appears to preclude oxygen atom transfer to it.[4] The principal orbital interaction in the transition state is a donor−acceptor interaction between the lone pair on phosphorus and the lowest-lying metal−oxygen $\pi^*$ orbital, so the reaction is well described as a nucleophilic attack of the phosphine at oxygen. This is consistent with substituent studies, where electron-donating substituents on triarylphosphines[5−10] and electron-withdrawing substituents on metal oxo complexes[11−15] lead to enhanced rates. Even oxo compounds that are capable of nucleophilic reactivity, such as complexation with Lewis acids, still display a preference for the oxidation of electron-rich phosphines.[16]

We recently reported the preparation and characterization of bis(iminoxolene)osmium oxo compounds ($^{R}$ap)$_2$OsO ($^{R}$ap = 2-(*p*-RC$_6$H$_4$N)-4,6-$^{t}$Bu$_2$C$_6$H$_2$O).[17] Structural and spectroscopic data indicate that the strong $\pi$ bonding of the metal to the oxo group precludes strong $\pi$ interactions with the iminoxolenes, which are well described as dianionic amidophenoxide ligands bonded to an osmium(VI) center. The modest $\pi$ donation of the amidophenoxides produces noticeable electronic anisotropy in the metal−oxo $\pi$ bonding, with the *B*-symmetry combination of amidophenoxide donor orbitals (known as the redox-active orbital or RAO of the iminoxolene ligand) interacting appreciably with the OsO $\pi^*$ orbital that runs from one amidophenoxide to the other but with the *A*-symmetry amidophenoxide combination precluded by symmetry from donating to an OsO $\pi^*$ orbital. This results

Received: January 8, 2021
Published: March 3, 2021

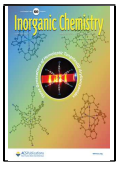


© 2021 American Chemical Society

https://dx.doi.org/10.1021/acs.inorgchem.1c00068
*Inorg. Chem.* 2021, 60, 4004–4014

in a nucleophilic face of the oxo ligand (where the oxygen p orbital contributes significantly to the HOMO, Figure 1a) and

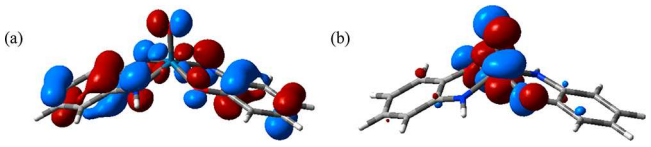


**Figure 1.** Bonding anisotropy in the oxo group in $(C_6H_4[NH]\text{-}O)_2OsO$. (a) HOMO, oriented roughly parallel to the line connecting the centers of the two iminoxolene ligands. (b) LUMO, oriented roughly perpendicular to the line connecting the centers of the two iminoxolene ligands.

an electrophilic face of the oxo ligand (where the OsO $\pi^*$ orbital does not interact with the iminoxolene $\pi$ orbitals, Figure 1b). Some nucleophilic reactivity of the oxo groups (reaction with $Me_3SiCl$ or $PCl_5$ to form osmium dichloride complexes) was described.

Here we describe the reactivity of oxobis(iminoxolene)-osmium complexes with triarylphosphines, tricyclohexylphosphine, and triarylphosphites. The compounds are cleanly deoxygenated to form reduced $(^{R}ap)_2Os(PR'_3)_n$ adducts in which the net reduction is accompanied by partial oxidation of the iminoxolene ligands. Varying the substituents on both the metal oxo compound and on the triarylphosphine results in little change in reactivity, painting a picture of a remarkably amphiphilic metal oxo group.

## RESULTS

**Scope of OAT Reactions of Oxobis(iminoxolene) osmium Complexes.** The treatment of oxobis(iminoxolene) complex $(^{H}ap)_2OsO$ with triphenylphosphine results in the rapid (minutes at room temperature) formation of 1 equiv of triphenylphosphine oxide and the formation of a mixture of green monophosphine complex $(^{H}ap)_2Os(PPh_3)$ and brown bis(phosphine) complex *trans*-$(^{H}ap)_2Os(PPh_3)_2$ (eq 1). The

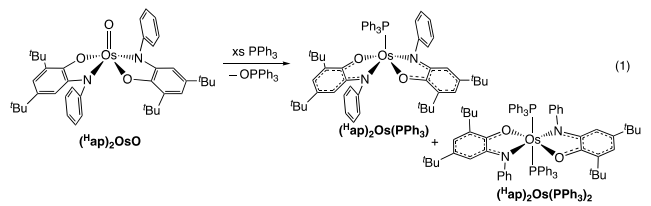


monophosphine complex precipitates from the reaction mixture if the reaction is carried out in dichloromethane with a stoichiometric amount of phosphine (2 equiv), while the bis(phosphine) adduct can be isolated if the reaction is carried out with excess $PPh_3$. Both compounds are diamagnetic by NMR, and $^{31}P$ NMR spectroscopy indicates that they are in rapid exchange with each other (and with free $PPh_3$) at room temperature. Para-substituted triarylphosphines behave similarly to $PPh_3$, but bulkier triarylphosphines such as tri-*o*-tolylphosphine and trimesitylphosphine do not react with $(^{H}ap)_2OsO$, even upon heating.

Other phosphorus(III) reagents also deoxygenate $(^{H}ap)_2OsO$. Tricyclohexylphosphine reacts more slowly than $PPh_3$ (over the course of an hour at 50 °C) to give $OPCy_3$ and the monophosphine adduct $(^{H}ap)_2Os(PCy_3)$ (eq 2). There is no evidence of the formation of a bis(phosphine) adduct by UV−visible or NMR spectroscopy. The observation of sharp,

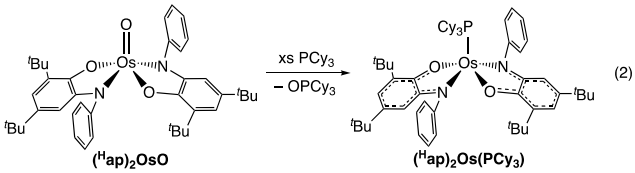


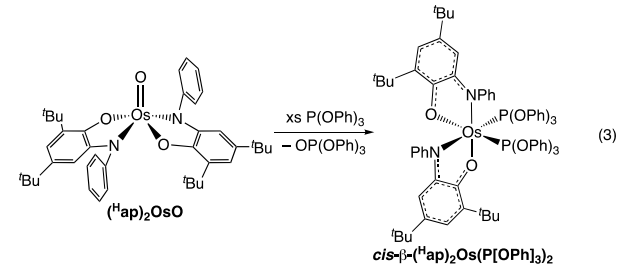


distinct signals in the $^{31}P$ NMR for $(^{H}ap)_2Os(PCy_3)$ and free $PCy_3$ indicates that the formation of a bis(phosphine) adduct is not only thermodynamically unfavorable but also kinetically slow at ambient temperature. Triphenylphosphite is more reactive than triphenylphosphine, reacting to form triphenylphosphate within seconds at room temperature. In this case, the diamagnetic product has two inequivalent, mutually coupled doublets ($\delta$ 58.0, 50.8, $J$ = 62 Hz) in the $^{31}P\{^{1}H\}$ NMR, indicating the exclusive formation of the unsymmetrical bis(phosphite) adduct *cis*-$\beta$-$(^{H}ap)_2Os(P[OPh]_3)_2$ (eq 3). The bulkier tri-*o*-tolylphosphite reacts more slowly but gives principally the analogous product, as judged by its $^{31}P$ NMR spectrum (Figure S1, $\delta$ = 57.4, 53.2, with both signals broadened, likely due to exchange with free $P(O\text{-}o\text{-}Tol)_3$). An additional singlet in the $^{31}P$ NMR ($\delta$ 50.7) indicates that this species is accompanied by ∼10% of a symmetric isomer.

Species that form weaker bonds to oxygen than trivalent phosphorus do not react with $(^{H}ap)_2OsO$. Instead, the oxygen atom transfer reactions go in the reverse direction, with the oxygenated forms of the compounds being deoxygenated by $(^{H}ap)_2Os(PPh_3)_2$. Over the course of several days at room temperature, triphenylarsine oxide and diphenylsulfoxide are deoxygenated to give triphenylarsine and diphenylsulfide, respectively, with the osmium being converted to $(^{H}ap)_2OsO$ and the $Ph_3P$ being converted to $Ph_3PO$. 2,6-Lutidine-*N*-oxide is deoxygenated to give 2,6-lutidine at room temperature; pyridine-*N*-oxide is partially deoxygenated, but the reaction does not give full conversion because binding of the product pyridine to osmium eventually halts the reaction. Molecular oxygen reacts rapidly to give phosphine oxide and $(^{H}ap)_2OsO$. While interpreting these data in terms of the thermodynamic stability of the osmium−oxo bond is complicated by the binding and release of triphenylphosphine as deoxygenation takes place, the fact that $Ph_3AsO$ (As−O BDE = 103 kcal $mol^{-1}$)[1b] is deoxygenated indicates qualitatively that $(^{H}ap)_2OsO$ contains a relatively strong osmium−oxygen bond and is thus a thermodynamically weak oxidant.

**Structure and Bonding of Deoxygenated $(^{H}ap)_2OsL_n$ Compounds.** The solid-state structure of $(^{H}ap)_2Os(PPh_3)_2$ (Tables 1 and 2, Figure 2) confirms the trans stereochemistry of the compound. The intraligand bond distances of the iminoxolene ligands can be analyzed using established correlations to estimate the apparent degree of oxidation of the ligands, called the metrical oxidation state (MOS).[18] Strikingly, the intraligand bond distances in $(^{H}ap)_2Os(PPh_3)_2$ are consistent with substantial transfer of electron density to


https://dx.doi.org/10.1021/acs.inorgchem.1c00068
Inorg. Chem. 2021, 60, 4004−4014

**Table 1. X-ray Crystallography of *trans*-($^{H}$ap)$_2$Os(PPh$_3$)$_2$, *trans*-($^{H}$ap)$_2$Os(CNC$_6$H$_3$-2,6-Me$_2$)$_2$·2 CD$_2$Cl$_2$, *cis*-*β*-($^{H}$ap)$_2$Os(P[OPh]$_3$)$_2$·CH$_3$CN, and *cis*-*β*-($^{H}$ap)$_2$Os(P[O-*o*-Tol]$_3$)(NCCH$_3$)·CD$_2$Cl$_2$**

| | *trans*-($^{H}$ap)$_2$Os(PPh$_3$)$_2$ | *trans*-($^{H}$ap)$_2$Os(CNC$_6$H$_3$-2,6-Me$_2$)$_2$·2CD$_2$Cl$_2$ | *cis*-*β*-($^{H}$ap)$_2$Os(P[OPh]$_3$)$_2$·CH$_3$CN | *cis*-*β*-($^{H}$ap)$_2$Os(P[O-*o*-Tol]$_3$) (NCCH$_3$)·CD$_2$Cl$_2$ |
|---|---|---|---|---|
| empirical formula | $C_{76}H_{80}N_2O_2OsP_2$ | $C_{60}H_{68}D_4Cl_4N_4O_2Os$ | $C_{78}H_{83}N_3O_8OsP_2$ | $C_{64}H_{74}D_2Cl_2N_3O_5OsP$ |
| temperature (K) | 120(2) | 120(2) | 120(2) | 120(2) |
| $\lambda$ (Å) | 0.71073 (Mo K$\alpha$) | 0.71073 (Mo K$\alpha$) | 0.71073 (Mo K$\alpha$) | 0.71073 (Mo K$\alpha$) |
| crystal system | triclinic | monoclinic | triclinic | triclinic |
| space group | $P\bar{1}$ | $P2_1/n$ | $P\bar{1}$ | $P\bar{1}$ |
| total data collected | 27 410 | 56 823 | 81 641 | 122 638 |
| no. of indep reflns | 7676 | 7276 | 17 718 | 29 715 |
| $R_{int}$ | 0.0442 | 0.0354 | 0.0460 | 0.0588 |
| obsd refls [$I > 2\sigma(I)$] | 7547 | 5823 | 15 752 | 22 297 |
| $a$ (Å) | 12.0659(7) | 11.520(7) | 11.804(2) | 10.3998(13) |
| $b$ (Å) | 12.3523(7) | 17.819(12) | 15.024(3) | 24.486(3) |
| $c$ (Å) | 12.5973(7) | 14.303(9) | 21.624(4) | 26.713(3) |
| $\alpha$ (deg) | 71.005(2) | 90 | 77.903(3) | 111.521(2) |
| $\beta$ (deg) | 69.696(2) | 95.141(9) | 77.677(3) | 97.431(2) |
| $\gamma$ (deg) | 62.731(2) | 90 | 68.709(3) | 102.177(2) |
| $V$ (Å$^3$) | 1533.63(15) | 2924(3) | 3454.0(12) | 6024.0(13) |
| $Z$ | 1 | 2 | 2 | 4 |
| $\mu$ (mm$^{-1}$) | 2.181 | 2.407 | 1.951 | 2.282 |
| crystal size (mm) | 0.14 × 0.14 × 0.13 | 0.26 × 0.19 × 0.13 | 0.29 × 0.15 × 0.07 | 0.14 × 0.11 × 0.07 |
| no. refined params | 536 | 466 | 1161 | 1461 |
| $R$ indices [$I > 2\sigma(I)$] | $R1$ = 0.0288, $wR2$ = 0.0518 | $R1$ = 0.0161, $wR2$ = 0.0359 | $R1$ = 0.0280, $wR2$ = 0.0615 | $R1$ = 0.0393, $wR2$ = 0.0893 |
| $R$ indices (all data) | $R1$ = 0.0299, $wR2$ = 0.0523 | $R1$ = 0.0258, $wR2$ = 0.0391 | $R1$ = 0.0359, $wR2$ = 0.0641 | $R1$ = 0.0657, $wR2$ = 0.0979 |
| goodness of fit | 1.030 | 1.043 | 1.028 | 1.031 |

**Table 2. Selected Bond Distances (Å), Metrical Oxidation States (MOS), and Angles (deg) for *trans*-($^{H}$ap)$_2$Os(PPh$_3$)$_2$, *trans*-($^{H}$ap)$_2$Os(CNC$_6$H$_3$-2,6-Me$_2$)$_2$·2CD$_2$Cl$_2$, *cis*-*β*-($^{H}$ap)$_2$Os(P[OPh]$_3$)$_2$·CH$_3$CN, and *cis*-*β*-($^{H}$ap)$_2$Os(P[O-*o*-Tol]$_3$)(NCCH$_3$)·CD$_2$Cl$_2$**

| | *trans*-($^{H}$ap)$_2$Os(PPh$_3$)$_2$ | *trans*-($^{H}$ap)$_2$Os (CNC$_6$H$_3$-2,6-Me$_2$)$_2$·2CD$_2$Cl$_2$ | *cis*-*β*-($^{H}$ap)$_2$Os(P[OPh]$_3$)$_2$·CH$_3$CN | | *cis*-*β*-($^{H}$ap)$_2$Os(P[O-*o*-Tol]$_3$)(NCCH$_3$)·CD$_2$Cl$_2$ | |
|---|---|---|---|---|---|---|
| | $n$ = 1 | $n$ = 1 | $n$ = 1 | $n$ = 2 | $n$ = 1, 3[a] | $n$ = 2, 4[a] |
| Os−O$n$ | 2.0537(14) | 2.0582(15) | 2.0719(15) | 2.0306(16) | 2.061(3) | 2.028(3) |
| Os−N$n$ | 1.9972(17) | 2.0238(17) | 2.0142(19) | 2.0590(18) | 1.990(5) | 1.988(3) |
| Os−P$n$ | 2.4199(6) | | 2.2330(7) | 2.2746(7) | 2.216(2) | |
| Os−C30 | | 2.0126(19) | | | | |
| C30−N30 | | 1.157(2) | | | | |
| Os−NCMe | | | | | | 2.069(6) |
| O$n$−C$n$1 | 1.328(2) | 1.3268(19) | 1.314(3) | 1.331(3) | 1.324(5) | 1.336(5) |
| N$n$−C$n$2 | 1.390(3) | 1.391(2) | 1.394(3) | 1.380(3) | 1.398(6) | 1.401(6) |
| C$n$1−C$n$2 | 1.413(3) | 1.417(2) | 1.428(3) | 1.427(3) | 1.415(5) | 1.412(7) |
| C$n$2−C$n$3 | 1.393(3) | 1.415(2) | 1.408(3) | 1.416(3) | 1.405(6) | 1.403(7) |
| C$n$3−C$n$4 | 1.379(3) | 1.377(2) | 1.377(3) | 1.387(3) | 1.380(11) | 1.380(6) |
| C$n$4−C$n$5 | 1.395(3) | 1.418(2) | 1.419(3) | 1.412(3) | 1.412(10) | 1.409(12) |
| C$n$5−C$n$6 | 1.390(3) | 1.393(2) | 1.378(3) | 1.385(3) | 1.381(7) | 1.387(5) |
| C$n$6−C$n$1 | 1.415(3) | 1.426(2) | 1.428(3) | 1.419(3) | 1.417(6) | 1.410(6) |
| MOS | −1.59(9) | −1.44(10) | −1.33(12) | −1.43(6) | −1.50(11) | −1.63(9) |
| O$n$−Os−N$n$ | 77.68(6) | 78.17(6) | 79.33(7) | 79.44(7) | 79.8(2) | 79.58(13) |
| P1−Os−P2 | 180.0 | | 87.28(2) | | | |
| Os−C30−N30 | | 174.17(14) | | | | |
| Os−N5−C1 | | | | | 164.3(4) | |

[a]Values given are the averages of chemically equivalent distances in the two crystallographically distinct molecules. The given esd's combine the variance of the independent values with the esd's of each individual observation.

the osmium, MOS = −1.59(9). These are more oxidized ligands than are found in oxobis(iminoxolene)osmium compounds, which have ligands that are structurally indistinguishable from fully reduced amidophenoxides. No crystal structure of ($^{H}$ap)$_2$OsO is available, but the MOS of linked bis(amidophenoxide) complex (Egan)OsO, which is spectroscopically very similar to unlinked ($^{R}$ap)$_2$OsO, has a ligand MOS = −1.98(12),[17] and DFT calculations on (ap)$_2$OsO (ap


https://dx.doi.org/10.1021/acs.inorgchem.1c00068
Inorg. Chem. 2021, 60, 4004−4014

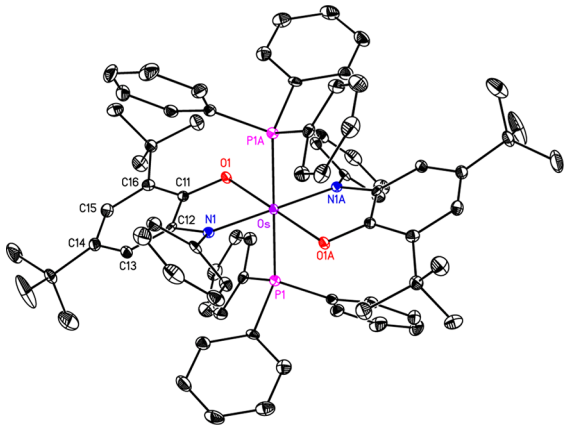


**Figure 2.** Thermal ellipsoid plot of *trans*-($^{H}$ap)$_2$Os(PPh$_3$)$_2$, with hydrogen atoms omitted for clarity.

= 1,2-OC$_6$H$_4$NH) give MOS = −1.92(6). In other words, two-electron reduction of the ($^{H}$ap)$_2$OsO complex is accompanied by a roughly one-electron oxidation of the iminoxolene ligands! This phenomenon is reproduced in DFT calculations on (ap)$_2$Os(PMe$_3$)$_2$, MOS = −1.37(7). The five-coordinate monophosphine complex is calculated to be similar, with (ap)$_2$Os(PMe$_3$) having an average MOS = −1.42(5).

While the apparent ligand oxidation is perplexing when viewed from a redox perspective, it makes perfect sense when viewed through the lens of $\pi$ bonding. The amidophenoxides in the square-pyramidal oxo complex are not strong $\pi$ donors because they do not compete effectively with the $\pi$ donor oxo ligand.[17] The Os═O $\pi^*$ orbitals are high in energy, so the energy match with the amidophenoxide redox-active orbital (RAO) is poor. Once (ap)$_2$OsO is deoxygenated, the osmium d$\pi$ orbitals fall in energy and the interaction of the $B_g$ combination of RAOs in (ap)$_2$Os(PR$_3$)$_2$ with the d$_{xz}$ orbital becomes quite strong. (The LUMO in Figure 3 is the

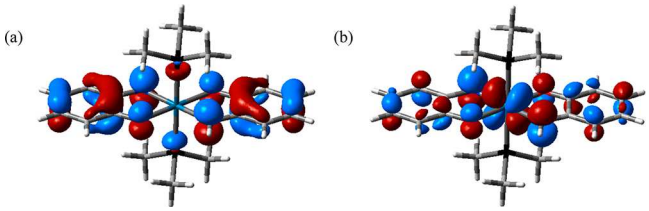


**Figure 3.** Calculated frontier Kohn−Sham orbitals of *trans*-(C$_6$H$_4$[NH]O)$_2$Os(PMe$_3$)$_2$. (a) HOMO and (b) LUMO.

antibonding component of this interaction.) Indeed, studies of other osmium and ruthenium iminoxolenes (without strongly $\pi$-bonding ancillary ligands) have concluded that the metal-iminoxolene $\pi$ bonding involves nearly equal sharing of electrons.[19] The $A_u$ combination has no overlap with the d orbitals and remains purely ligand-centered (Figure 3, HOMO). The average of one fully ligand-centered RAO (MOS = −2) and one highly covalent RAO (MOS ≈ −1) predicts that the product should have an MOS close to −1.5, as observed for ($^{H}$ap)$_2$Os(PPh$_3$)$_2$ as well as for isoelectronic (Clip)Os(py)$_2$ (MOS = −1.68(13)).[19] Put succinctly, the apparent oxidation of the ligands on reduction of (ap)$_2$OsO to (ap)$_2$Os(PPh$_3$)$_2$ is due to a change in the metal−iminoxolene $\pi$ bond order from 0 in the oxo complex to 0.5 in the *trans*-diphosphine complex.

The cis geometry of ($^{H}$ap)$_2$Os(P[OPh]$_3$)$_2$ implied by the presence of inequivalent, mutually coupled phosphorus atoms in its $^{31}$P NMR spectrum is confirmed by X-ray crystallography (Figure 4). A *cis*-bis(iminoxolene)osmium complex with

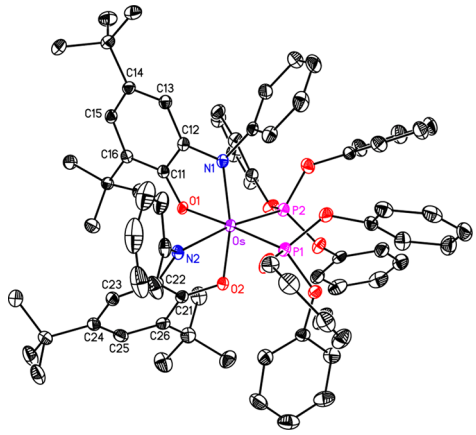


**Figure 4.** Thermal ellipsoid plot of *cis*-$\beta$-($^{H}$ap)$_2$Os(P[OPh]$_3$)$_2$·CH$_3$CN, with hydrogen atoms and the lattice solvent omitted for clarity.

neutral donors (intramolecularly coordinated thioethers), Os(L$_{N,O,S}$)$_2$, has been prepared,[20] and *cis*-bis(iminoxolene)-ruthenium complexes with neutral donors are also known.[21,22] In the trans geometry, the inversion center means that the ungerade ligand-centered combination is strictly nonbonding, giving rise to two filled d$\pi$ nonbonding orbitals, one filled metal−ligand $\pi$ bonding orbital, and one filled ligand-centered nonbonding orbital in the metal complex. In contrast, in the $C_2$- or pseudo-$C_2$ symmetry of the cis geometry, the d$\pi$ orbitals transform as 2$A$ + $B$, so both combinations of the ligand RAOs can interact with the d$\pi$ orbitals.[23] This would be expected to give rise to two filled metal−ligand $\pi$ bonding orbitals, one filled nonbonding d$\pi$ orbital, and one filled metal−ligand $\pi^*$ orbital.

While this leads to the same net $\pi$ bond order as the trans geometry, DFT calculations on (ap)$_2$Os(P[OMe]$_3$)$_2$ (Figure 5), consistent with those on isoelectronic Os(L$_{N,O,S}$)$_2$,[20] do not

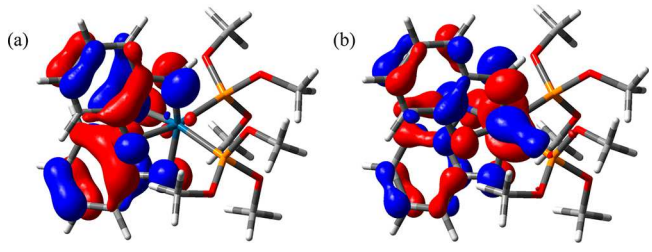


**Figure 5.** Calculated frontier Kohn−Sham orbitals of *cis*-$\beta$-(C$_6$H$_4$[NH]O)$_2$Os(P[OMe]$_3$)$_2$. (a) HOMO and (b) LUMO.

support the characterization of the HOMO as metal−ligand antibonding. Instead, the HOMO, which is antisymmetric with respect to the pseudo-2-fold axis, is essentially completely ligand-centered and thus nonbonding. The cis and trans isomers thus have similar electronic structures. This is borne out by their similar optical spectra, which are dominated by very intense transitions in the red ($\lambda_{max}$ = 917 nm for *trans*-($^{H}$ap)$_2$Os(PPh$_3$)$_2$, 950 nm for *cis*-$\beta$-($^{H}$ap)$_2$Os(P[OPh]$_3$)$_2$),


https://dx.doi.org/10.1021/acs.inorgchem.1c00068
Inorg. Chem. 2021, 60, 4004−4014

assigned (with the aid of TDDFT calculations) to HOMO → LUMO transitions.

Careful inspection of the structures of *cis*-$(ap)_2OsX_2$ complexes indicates that the compounds with neutral donors adopt conformations where the iminoxolene ligands are twisted so as to minimize their interactions with the metal *B*-symmetry d$\pi$ orbital (Figure 6). As the X−Os−N−C2

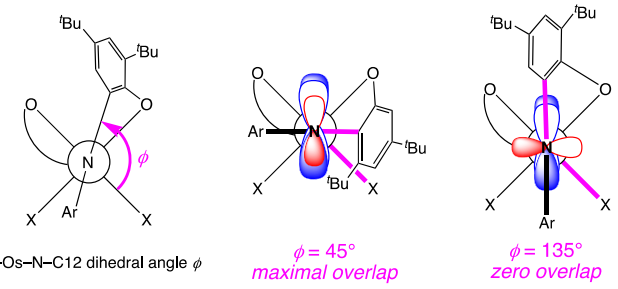


**Figure 6.** Effect of the iminoxolene−osmium dihedral angle on $\pi$ overlap in *cis*-$(ap)_2OsX_2$.

dihedral angle $\phi$ (or the analogous X−Os−O−C1 dihedral if the ligand is bound with O axial) increases, the p$\pi$ orbital on the axial donor pivots in such a way as to decrease the overlap with the osmium *B*-symmetry d$\pi$ orbital. (The equatorial donors on the iminoxolenes have essentially no overlap with this d$\pi$ orbital regardless of conformation.) With $\phi$ = 135°, there is no overlap between these orbitals, while $\phi$ = 45° corresponds to maximum overlap. In *cis*-*β*-$(^{H}ap)_2Os(P[OPh]_3)_2$, with dihedral angles of 122.2° (axial O) and 109.1° (axial N), there is expected to be little iminoxolene−osmium overlap, and hence the ligand-centered HOMO is essentially nonbonding. These dihedral angles are reproduced in DFT calculations on *cis*-*β*-$(ap)_2Os(P[OMe]_3)_2$ (axial O, $\phi$ = 109.4°; axial N, $\phi$ = 112.8°). The mono-tri-*o*-tolylphosphite complex *cis*-*β*-$(^{H}ap)_2Os(P[O\text{-}o\text{-}Tol]_3)(NCCH_3)$, which crystallizes from a solution of the bis(phosphite) complex layered with acetonitrile (Figure S2), shows average dihedral angles of $\phi$ = 125.9° (axial O) and 91.8° (axial N). Large dihedral angles are observed in $Os(L_{N,O,S})_2$ ($\phi$ = 117.7°, 118.9°)[20] as well as in isoelectronic ruthenium complexes such as $(ap)_2Ru(bpy)$ (three examples, avg $\phi$ = 121.5°).[21]

These large dihedral angles are not merely an intrinsic structural bias of the *cis*-bis(iminoxolene) fragment because they change substantially as the electronic structure of the metal complex changes. For example, in *cis*-*α*-$(^{H}ap)_2OsCl_2$, with two fewer $\pi$ electrons than in $(^{H}ap)_2OsL_2$, the *B*-symmetry $\pi$ orbitals need to accommodate only two (rather than four) electrons, and the complex is expected to have a filled $\pi$ bonding and empty $\pi^*$ orbital of this symmetry. This is in agreement with the ligand bond lengths and DFT calculations on this complex, which show strong osmium−iminoxolene $\pi$ interactions involving these orbitals. Here, where the $\pi$ overlap is energetically favorable, the complex adopts a conformation with a drastically smaller dihedral angle ($\phi$ = 68.3°).[17] Similar angles are observed in *cis*-*β*-$(Clip)OsCl_2$ (67.6 and 69.7°),[19] *cis*-*α*-$(^{H}ap)_2Os(OCH_2CH_2O)$ (67.8 and 68.2°),[17] and ruthenium complex $(^{H}ap)(PhNHC_6H_4NH)RuCl_2$ (77.6°).[24] The shift from a repulsive filled−filled $\pi$ interaction to a favorable filled−empty $\pi$ interaction thus results in a conformational shift in the ligand dihedral angle of about 50°.

The phosphite complex has slightly more positive MOS values than does the phosphine complex. While this might be due to differences in bonding between the cis and trans geometries, it is more likely due to the greater $\pi$-acceptor capabilities of the phosphite ligands. Consistent with this, isonitrile complex *trans*-$(^{H}ap)_2Os(CNC_6H_3\text{-}2,6\text{-}Me_2)_2$, crystallized from the reaction of *trans*-$(^{H}ap)_2Os(PPh_3)_2$ and xylyl isonitrile (Table 1, Figure S3), has an MOS value of −1.44(10) (Table 2), similar to those in the *cis*-bis(phosphite) compound. Analogously, *cis*-*β*-$(^{H}ap)_2Os(P[O\text{-}o\text{-}Tol]_3)(NCCH_3)$, where one $\pi$-acceptor phosphite has been replaced by acetonitrile, has a more negative MOS (−1.57 avg) than the bis(phosphite) complex, similar to the trans bis(phosphine) complex.

**Kinetics of Oxygen Atom Transfer Reactions.** The reaction of triphenylphosphine with brown oxo complex $(^{H}ap)_2OsO$ to form a mixture of $(^{H}ap)_2Os(PPh_3)$ ($\lambda_{max}$ = 654 nm) and $(^{H}ap)_2Os(PPh_3)_2$ ($\lambda_{max}$ = 917 nm) can be monitored by optical spectroscopy (Figure 7). The observation

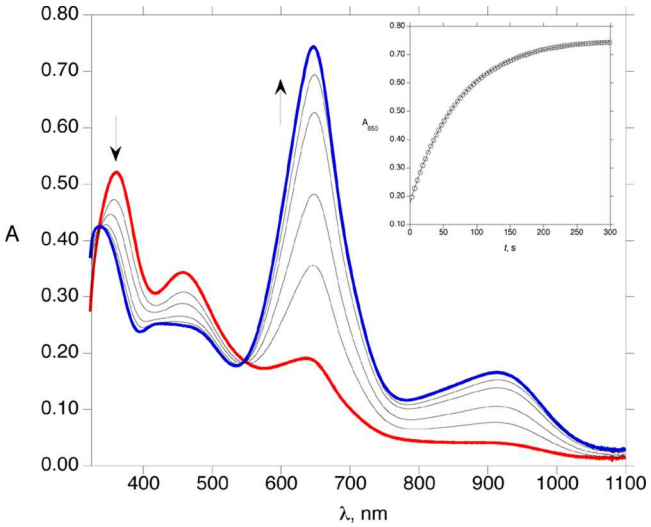


**Figure 7.** Successive optical spectra for the reaction of $(^{H}ap)_2OsO$ ($3.42 \times 10^{-5}$ M) with $PPh_3$ (0.0327 M) in $CH_2Cl_2$ at 23 °C. Spectra are shown at $t$ = 2 (red), 27, 55, 111, 165, and 275 s (blue). Inset: $A_{650}$ as a function of time. The solid line is a fit to exponential decay.

of an isosbestic point confirms that the reaction cleanly produces the two phosphine adducts in their equilibrium ratio, and the absorbance changes over time in the presence of excess phosphine conform to exponential decay (Figure 7 inset). Increasing the concentration of phosphine causes an enhancement of the 917 nm absorption at the expense of the 654 nm absorption as the product equilibrium increasingly favors $(^{H}ap)_2Os(PPh_3)_2$, and a linear increase in $k_{obs}$ with increasing $[PPh_3]$ is observed (Figure S4). These data indicate that the reaction is first order in both $(^{H}ap)_2OsO$ and in $PPh_3$, with an overall second-order rate constant of 0.57(6) L $mol^{-1}$ $s^{-1}$ ($CH_2Cl_2$, 23 °C). Entirely analogous behavior is observed in reactions of $(^{H}ap)_2OsO$ with para-substituted triarylphosphines $P(C_6H_4X)_3$ (X = $CH_3$, Cl, $CH_3O$, and $CF_3$; Figure S4) and in reactions of iminoxolene complexes $(^{R}ap)_2OsO$ substituted in the para position of the *N*-phenyl group (R = $CH_3O$, $CH_3S$, or $CF_3$) with $PPh_3$ (Figure S5).

Reactions of $(^{R}ap)_2OsO$ with tri−*ortho*-tolylphosphite take a different kinetic course, with the absorbances at long wavelength showing a rapid rise followed by a slower fall, consistent with the formation of a long-lived intermediate in


https://dx.doi.org/10.1021/acs.inorgchem.1c00068
Inorg. Chem. 2021, 60, 4004−4014

this reaction. An inspection of the optical spectra taken at time points near the maximum in absorbance (Figure 8), where the

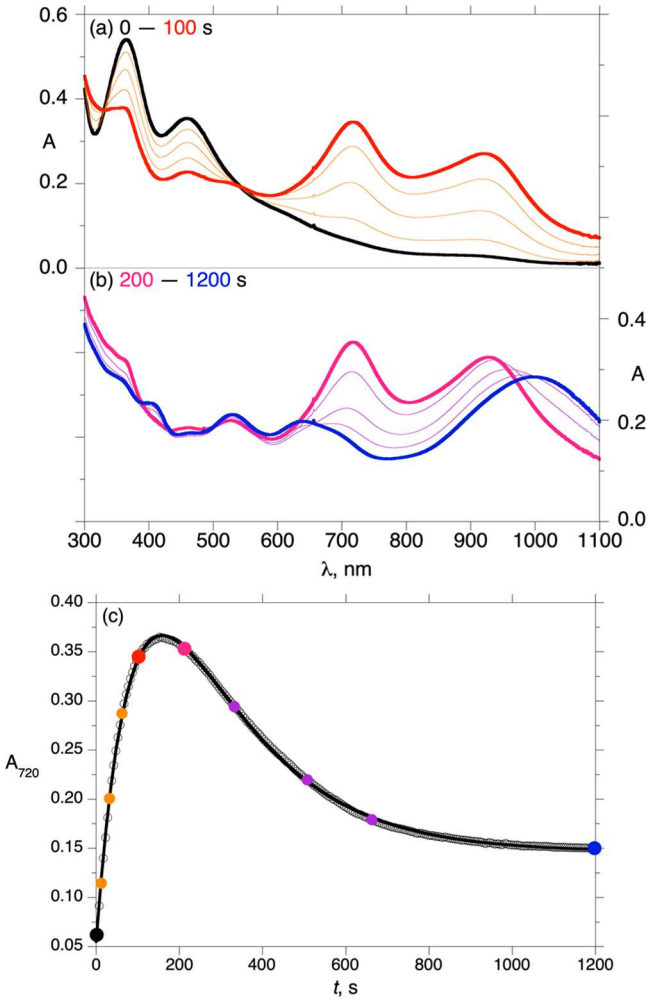


**Figure 8.** UV−visible monitoring of the reaction of $(^{H}ap)_2OsO$ (3.28 × $10^{-5}$ M) with P(O-*o*-Tol)$_3$ (2.37 × $10^{-3}$ M) in $CH_2Cl_2$ at 22.4 °C. (a) Successive optical spectra from 0 to 100 s. (b) Successive optical spectra from 200 to 1200 s. (c) $A_{720}$ as a function of time. The solid line is a fit to successive irreversible pseudo-first-order reactions. The highlighted time points correspond to the spectra in (a) and (b).

intermediate is near its maximal concentration, show a marked resemblance to those shown by the equilibrium mixture of $(^{R}ap)_2Os(PAr_3)$ and *trans*-$(^{R}ap)_2Os(PAr_3)_2$ that is formed in the reaction of triarylphosphines with $(^{R}ap)_2OsO$. The initial phase of the reaction is thus assigned to the oxidation of phosphite to phosphate, with the initial formation of rapidly equilibrating $(^{R}ap)_2Os(P[O\text{-}o\text{-}Tol]_3)$ and *trans*-$(^{R}ap)_2Os(P[O\text{-}o\text{-}Tol]_3)_2$, followed by subsequent slower isomerization to the final product, *cis*-*β*-$(^{R}ap)_2Os(P[O\text{-}o\text{-}Tol]_3)_2$. While the dependence of $k_{2(obs)}$ on $[P(OAr)_3]$ is complex, $k_{1(obs)}$ is linearly dependent on phosphite concentration (Figure S6), and the second-order rate constant $k_1$ is thus assigned to the direct oxygen atom transfer reaction of phosphite with the osmium−oxo group to give the phosphate complex, which is displaced rapidly by phosphite (Scheme 1). Triphenylphosphite shows a similar time course in its reactions with $(^{H}ap)_2OsO$, but with a rate constant for atom transfer that is an order of magnitude faster than that shown by the bulkier tri(*o*-tolyl)phosphite (82(8) vs 4.66(6) L mol$^{-1}$ s$^{-1}$).

## DISCUSSION

The accepted mechanism for oxygen atom transfer between metal oxo complexes and phosphorus(III) reagents involves the direct attack of $R_3P$ on the oxygen atom of the metal oxo complex to form an intermediate $M(OPR_3)$ complex.[2,3,5] While this intermediate is not observed in reactions of $(^{R}ap)_2OsO$ with $R_3P$, presumably due to rapid displacement of the weakly binding phosphorus(V) compound by phosphine or phosphite, all other experimental data are in agreement with this mechanism. For example, reactions are uniformly first order in osmium and first order in $PR_3$, with increases in the steric bulk of the phosphine or phosphite resulting in significant decreases in the reaction rate. DFT calculations find a transition state for the addition of $PMe_3$ to $(ap)_2OsO$ (Figure 9) with $\Delta G^{‡}$ = 22.4 kcal mol$^{-1}$, in qualitative agreement with the observed $\Delta G^{‡}$ = 17.7 kcal mol$^{-1}$ for the reaction of $PPh_3$ with $(^{H}ap)_2OsO$. Reaction to form the phosphine oxide adduct is calculated to be exoergic by 8.5 kcal mol$^{-1}$ (calculated $\Delta H°$ = −20.2 kcal mol$^{-1}$), and the displacement of $OPMe_3$ by $PMe_3$ is calculated to be exoergic by 14.9 kcal mol$^{-1}$.

The phosphine is calculated to approach the oxo group almost directly over the osmium−iminoxolene oxygen bond (O2−Os−O−P dihedral angle of 0.6°). This is well aligned with the complex's LUMO (Figure 1), consistent with a reaction that, at least computationally, involves some degree of donation of the phosphorus lone pair to the osmium−oxo $\pi^*$ orbital. This result suggests that the iminoxolene-induced anisotropy in the metal−oxo bond, previously observed spectroscopically,[17] may have consequences in chemical reactions.

The geometry at phosphorus in the transition state resembles a sawhorse much more than a tetrahedron (e.g., O−P−C32 angle of 150.2°). This geometry has been observed in calculations on the addition of phosphines to a terminal iron nitride, where it was interpreted as evidence of the nucleophilic character of the nitride in the atom-transfer reaction, consistent with Hammett studies indicating faster reactions of electron-poor triarylphosphines.[25] However, sawhorse-like geometry has also been seen in calculations on reactions of phosphines with dioxomolybdenum(VI) compounds,[2] which are experimentally electrophilic at oxygen,[11,14,15] so this phenomenon may be an artifact of the generally early transition states of these highly exothermic reactions.

Experimentally, the rate of reaction of $(^{R}ap)_2OsO$ with phosphorus(III) reagents is remarkably insensitive to substituent effects on either the metal complex or on the phosphine, with no trend in the reaction rate with the Hammett substituent constant (Figure 10). Both electron-donating and electron-withdrawing substituents (on either the ligand or the phosphine) increase the reaction rate relative to hydrogen, but the effects are universally small. All second-order rate constants for reactions with triarylphosphines, for example, are within a factor of 3.6 of the rate constant for the reaction of $(^{H}ap)_2OsO$ with $PPh_3$. The observed lack of correlation of OAT rates with substituents on triarylphosphines is unprecedented; all previous reactions have shown faster reactions with more electron-donating substituents, though previously observed effects have often been modest.[5−10] Since phosphites are more electron-poor than phosphines, one might have expected them to behave more electrophilically toward a nucleophilic metal oxo complex, but if anything, the reverse is


https://dx.doi.org/10.1021/acs.inorgchem.1c00068
Inorg. Chem. 2021, 60, 4004−4014

**Scheme 1. Proposed Reaction Mechanism of $(^{H}ap)_2OsO$ with $P(OAr)_3$**

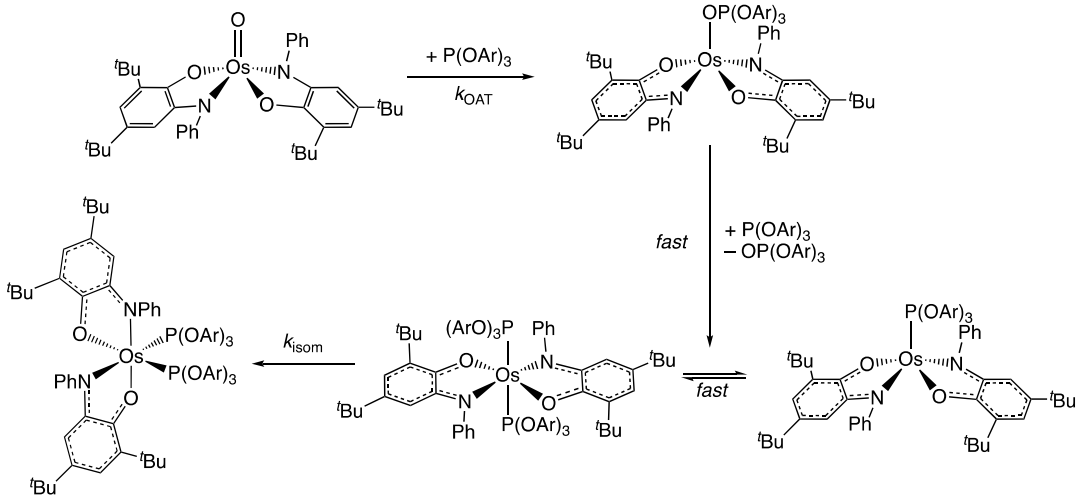


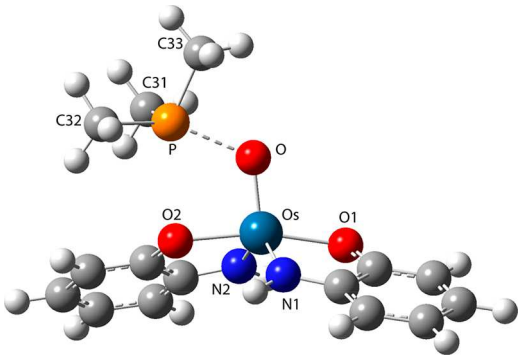


**Figure 9.** Transition state for oxygen atom transfer from $(ap)_2OsO$ to $PMe_3$ as calculated by DFT (B3LYP, SDD basis for Os, 6-31G* for all other atoms). Selected bond distances (Å): Os–O, 1.786; Os–O1, 2.035; Os–O2, 2.039; Os–N1, 1.919; Os–N2, 1.926; P–O, 2.149. Selected bond angles (deg): N1–Os–N2, 125.7; O1–Os–O2, 166.5; Os–O–P, 119.6; O–P–C32, 150.2. MOS: ring 1, −1.80(6); ring 2, −1.87(4).

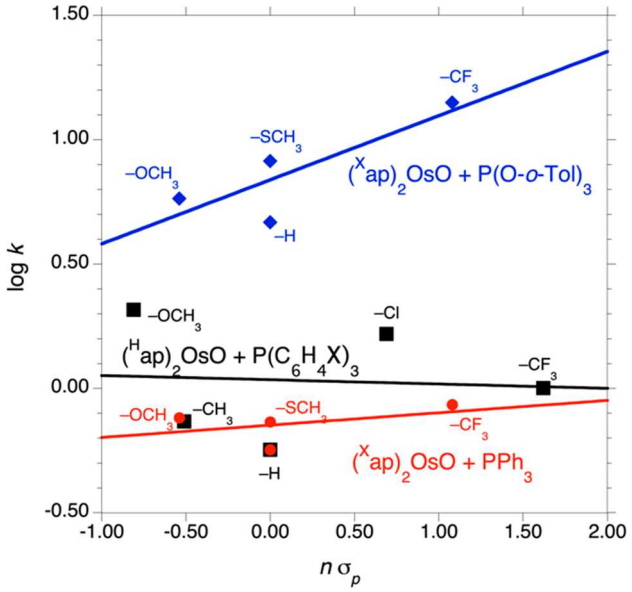


**Figure 10.** Hammett plot for the reaction of $(^{X}ap)_2OsO$ with $PPh_3$ (log $k$ vs $2\sigma_p$, red ●), the reaction of $(^{H}ap)_2OsO$ with $P(C_6H_4–X)_3$ (log $k$ vs $3\sigma_p$, ■), and the reaction of $(^{X}ap)_2OsO$ with $P(O\text{-}o\text{-}Tol)_3$ (log $k$ vs $2\sigma_p$, blue ♦).

observed here, with the Hammett plot for the reaction of P(O-*o*-Tol)$_3$ with $(^{X}ap)_2OsO$ showing the steepest positive slope (though still very small, $\rho$ = 0.26(12)).

Apparently, oxygen atom transfer from osmium to phosphorus involves similar amounts of (back)-donation from oxygen to phosphorus as it does donation from phosphorus to oxygen. Consistent with this, the rates of oxygen atom transfer correlate inversely with the HOMO–LUMO gaps in the oxo complexes (Figure 11), as gauged by the energy of the longest-wavelength optical transition, though the effect is again small, as it must be given the modest total spread in reaction rates. It has been observed that optical transitions in amidophenoxide complexes are not well correlated with the electron-donating or -accepting character of the *N*-aryl substituents.[26] The fact that OAT reaction rates correlate better with the optical bands than the Hammett constants suggests that the combination of the ability to accept electrons from the phosphorus (associated with a low-lying LUMO, Figure 1b) with the ability to donate electrons from oxygen to phosphorus (associated with a high-lying HOMO, Figure 1a) is what governs the rate rather than one effect dominating the other.

Why do bis-iminoxolene complexes $(^{X}ap)_2OsO$ show a balance between electrophilic and nucleophilic character in their reactions with phosphines, where previously studied metal–oxo complexes have acted predominantly as electrophiles? A plausible explanation arises from the increasing degree of $\pi$ donation from the iminoxolenes as the atom transfer proceeds, as witnessed by the striking increase in the apparent oxidation state of the iminoxolenes in the deoxygenated products compared to the reactants. This trend is partially realized in the transition state (calculated average MOS = −1.84(5)). The increase in $\pi$ donation from the iminoxolenes as the reaction proceeds means that the transition state is expected to be better stabilized by more electron-rich ligands, which predicts an atypically rate-accelerating effect of electron-donating substituents on the metal complex. Since the iminoxolene–osmium $\pi$-donor interaction has metal–oxo $\pi^*$ character (Figure 1a), the oxo group is expected to develop more electron density in the


https://dx.doi.org/10.1021/acs.inorgchem.1c00068
Inorg. Chem. 2021, 60, 4004–4014

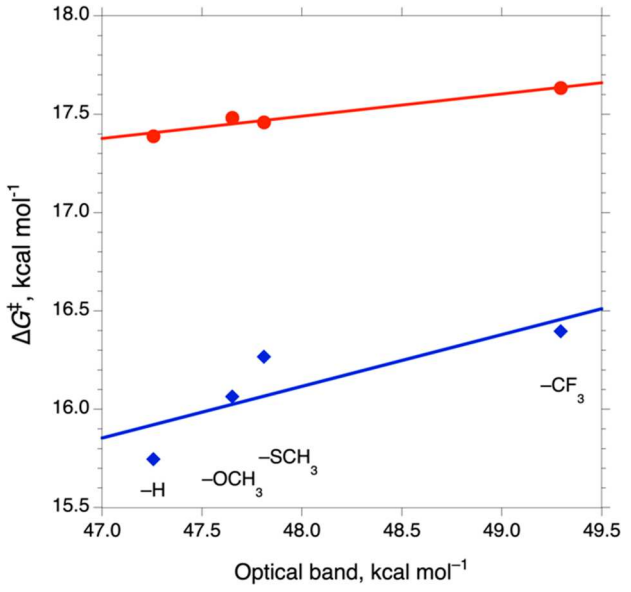


**Figure 11.** Correlation of the barrier to OAT with the energy of the long-wavelength optical band in reactions of $(^{X}ap)_2OsO$ with $PPh_3$ (red ●) and with $P(O\text{-}o\text{-}Tol)_3$ (blue ♦).

transition state compared to reactions of complexes with less electronically flexible ancillary ligands. This would enhance the importance of any back-donation to phosphorus in the transition state. Thus, in addition to the stereodirecting effects of the $\pi$-donor iminoxolene ligands, steering the substrate toward the LUMO located between the iminoxolene ligands, the iminoxolene $\pi$ donation also appears to affect the polarization of the transition state, rendering the oxo group amphiphilic.

## CONCLUSIONS

Bis-iminoxolene osmium−oxo compounds $(^{R}ap)_2OsO$ undergo rapid oxygen atom transfer reactions with phosphines and phosphites to form deoxygenated species $(^{R}ap)_2OsL_n$. Compounds with weaker bonds to oxygen than in $R_3PO$, such as sulfoxides and triphenylarsine oxide, are deoxygenated by $(^{R}ap)_2OsL_n$. In the reduced osmium complexes, one combination of $\pi$ orbitals on the iminoxolene ligands can engage in strong $\pi$ bonding with the osmium, resulting in the counterintuitive result that this two-electron reduction of the complexes results in an apparent oxidation of the ligands due to their enhanced ability to donate to the metal center. In *trans*-$(^{R}ap)_2OsL_2$, one ligand $\pi$ combination is strictly nonbonding by symmetry, while in *cis*-$(^{R}ap)_2OsL_2$, one ligand $\pi$ combination is rendered essentially nonbonding by twisting of the iminoxolene ligands. The electronic effects of substituents either on the iminoxolene ligand or on triarylphosphines on the kinetics of oxygen atom transfer are extremely small, contrasting with the more common observation of the electrophilic behavior of metal oxo complexes in their reactions with phosphines. The amphiphilic behavior of $(^{R}ap)_2OsO$ is consistent with the unusual ability of the iminoxolenes to $\pi$ donate to osmium.

## EXPERIMENTAL SECTION

Unless otherwise noted, procedures were carried out in an inert-atmosphere glovebox. Deuterated solvents were obtained from Cambridge Isotope Laboratories and were vacuum transferred from appropriate drying agents and then stored in the glovebox before use. $CD_2Cl_2$ was dried over molecular sieves and then $CaH_2$. Benzene-$d_6$ and toluene-$d_8$ were dried over sodium. Protio solvents were purchased as anhydrous grades from Acros, except for methanol, which was dried over 4 Å molecular sieves. Dry solvents were stored in the glovebox prior to use. NMR spectra were recorded on a Bruker Avance DPX 400 or 500 spectrometer. Chemical shifts for $^{1}H$ and $^{13}C\{^{1}H\}$ spectra are reported in ppm downfield from TMS, with spectra referenced using the known chemical shifts of the solvent residuals. $^{31}P\{^{1}H\}$ NMR spectra are reported in ppm downfield of external 85% $H_3PO_4$. Infrared spectra were measured on a Jasco-6300 FT-IR spectrometer as Nujol mulls pressed between NaCl plates. UV−visible−NIR spectra were recorded in 1 cm quartz cells on a Jasco V-670 spectrophotometer. Elemental analyses were performed by Robertson Microlit Laboratories (Ledgewood, NJ).

Oxobis(iminoxolene) complexes $(^{R}ap)_2OsO$ (R = H, $CH_3O$, $CH_3S$, and $CF_3$) were synthesized as described previously.[17] All other reagents were commercially available and were used as received.

**$(^{H}ap)_2Os(PPh_3)$.** In a 50 mL round-bottomed flask were combined 0.5047 g of $(^{H}ap)_2OsO$ (0.633 mmol), 0.3821 g of $PPh_3$ (1.45 mmol, 2.29 equiv), and 25 mL of $CH_2Cl_2$. The flask was stoppered and allowed to stir overnight. The dark-green solution was filtered on a glass frit, and the solid was washed with 2 × 2 mL $Et_2O$ followed by 1 × 1 mL $CH_2Cl_2$ to give 0.5957 g of (90%) $(^{H}ap)_2Os(PPh_3)$ as a dark-green solid, which was stored at −30 °C. $^{1}H$ NMR spectroscopy showed that the isolated material was contaminated with ∼2% $(^{H}ap)_2OsO$ and ∼2% $OPPh_3$, precluding satisfactory elemental analysis. $^{1}H$ NMR ($CD_2Cl_2$): $\delta$ 7.46 (t, 7.5 Hz, 4H, *m*-Ph of $^{H}ap$), 7.20 (t, 7.5 Hz, 3H, *p*-$PPh_3$), 7.12 (t, 7.5 Hz, 2H, *p*-Ph of $^{H}ap$), 7.06 (t, 7 Hz, 6H, *p*-$PPh_3$), 6.78 (d, 7 Hz, 6H, *o*-Ph of $^{H}ap$), 6.66 (dd, 12, 8 Hz, 6H, *o*-$PPh_3$), 6.63 (s, 4H, 3,5-H of $^{H}ap$), 1.40 (s, 18H, $^{t}Bu$), 1.30 (s, 18H, $^{t}Bu$). $^{13}C\{^{1}H\}$ NMR ($CD_2Cl_2$): $\delta$ 182.96 ($^{H}ap$ CO), 155.11, 154.93, 137.60 (d, $^{1}J_{PC}$ = 62 Hz, PC), 136.06, 133.77, 133.49 (d, $J_{PC}$ = 10 Hz), 131.57, 130.16, 128.23 (d, $J_{PC}$ = 11 Hz), 127.99, 126.72, 120.27, 112.88, 35.30 ($C(CH_3)_3$), 34.24 ($C(CH_3)_3$), 31.90 ($C(CH_3)_3$), 30.01 ($C(CH_3)_3$). $^{31}P\{^{1}H\}$ NMR (toluene-$d_8$): $\delta$ −47.50. IR (nujol mull, $cm^{-1}$): 3063 (w), 1588 (s), 1548 (m), 1484 (s), 1435 (s), 1301 (s), 1254 (s), 1232 (m), 1204 (s), 1165 (m), 1095 (s), 1073 (w), 1026 (m), 1001 (m). UV−vis−NIR ($CH_2Cl_2$): $\lambda_{max}$ = 359 nm ($\varepsilon$ = 14 000 L $mol^{-1}$ $cm^{-1}$), 471 nm (10 000), 654 nm (22 000), 975 nm (1200), 1220 nm (800).

***trans*-$(^{H}ap)_2Os(PPh_3)_2$.** A mixture of 0.1140 g of $(^{H}ap)_2OsO$ (0.143 mmol) and 0.1930 g of $PPh_3$ (0.736 mmol, 5.15 equiv) was stirred overnight in 2.5 mL of $CH_2Cl_2$. The dark-green solution was filtered through a glass frit, and the solid was washed with 3 × 3 mL $Et_2O$ and dried for 20 min to give 0.1640 g of *trans*-$(^{H}ap)_2Os(PPh_3)_2$ (88%). $^{1}H$ NMR ($CD_2Cl_2$): $\delta$ 7.40 (t, 7 Hz, 4H, *m*-Ph of $^{H}ap$), 7.25 (t, 7 Hz, 6H, *p*-$PPh_3$), 7.17 (t, 6.7 Hz, 12H, *m*-$PPh_3$), 7.06 (t, 7 Hz, 2H, *p*-Ph of $^{H}ap$), 6.95 (t, 8 Hz, 12H, *o*-$PPh_3$), 6.74 (d, 7 Hz, 4H, *o*-Ph of $^{H}ap$), 6.58 (s, 4H, 3,5-H of $^{H}ap$), 1.35 (s, 18H, $^{t}Bu$), 1.25 (s, 18H, $^{t}Bu$). $^{13}C\{^{1}H\}$ NMR ($CD_2Cl_2$): $\delta$ 183.25 ($^{H}ap$ CO), 155.36, 155.22, 137.67 (m, PC), 136.23, 133.95 (m), 131.74, 129.60 (m), 128.70 (m), 128.17, 126.87, 120.52, 113.17, 35.50 ($C(CH_3)_3$), 34.44 ($C(CH_3)_3$), 32.10 ($C(CH_3)_3$), 30.27 ($C(CH_3)_3$). $^{31}P\{^{1}H\}$ NMR ($CD_2Cl_2$): $\delta$ −28.77 (v br). IR (Nujol mull, $cm^{-1}$): 3054 (w), 1585 (m), 1571 (w), 1538 (m), 1395 (m), 1389 (m), 1378 (m), 1365 (m), 1293 (s), 1270 (w), 1256 (w), 1239 (s), 1200 (s), 1168 (m), 1088 (m), 1076 (w), 1024 (m), 1001 (m). Anal. Calcd for $C_{76}H_{80}N_2O_2OsP_2$: C, 69.91; H, 6.18; N, 2.15. Found: C, 69.76; H, 6.15; N, 2.23.

**$(^{H}ap)_2Os(PCy_3)$.** To a 20 mL scintillation vial was added 0.3563 g of $(^{H}ap)_2OsO$ (0.447 mmol), 0.2780 g of $PCy_3$ (0.991 mmol, 2.22 equiv), 7 mL of $C_6H_6$, and a stir bar. The vial was sealed with a Teflon-lined cap, taken out of the drybox, and stirred for 1.5 h in a 70 °C oil bath. The solution was cooled to room temperature and taken into the drybox, where the solution was filtered through a frit. The filtrate was collected, and the solvent was removed on a vacuum line. In the drybox, the residue was dissolved in 10 mL of methanol and the solution was placed in a clean scintillation vial. After standing for 3 days at room temperature, the mixture was filtered through a glass frit and the solid was washed with 2 × 3 mL of MeOH, furnishing 0.3983


https://dx.doi.org/10.1021/acs.inorgchem.1c00068
Inorg. Chem. 2021, 60, 4004−4014

g of ($^{H}$ap)$_2$Os(PCy$_3$) (84%). $^1$H NMR (C$_6$D$_6$): $\delta$ 7.35 (s, 2H, $^{H}$ap H-3 or -5), 7.13 (s, 2H, $^{H}$ap H-3 or -5), 7.12 (br s, 4H, *o*- or *m*-Ph), 7.01 (t, 7.2 Hz, 2H, *p*-Ph), 6.79 (v br, 4H, *o*- or *m*-Ph), 2.18 (q, 11.5 Hz, 3H, PCy$_3$), 1.90 (d, 11 Hz, 3H, PCy$_3$), 1.72 (obscured by $^t$Bu peak, 3H, PCy$_3$), 1.71 (s, 18H, $^t$Bu), 1.51 (d, 12 Hz, 3H, PCy$_3$), 1.46 (q, 12.5 Hz, 3H, PCy$_3$), 1.33 (m, 9H, PCy$_3$), 1.27 (s, 18H, $^t$Bu), 1.10 (q, 13 Hz, 3H, PCy$_3$), 1.02 (q, 12.5 Hz, 3H, PCy$_3$), 0.76 (q, 12.5 Hz, 3H, PCy$_3$). $^{13}$C{$^1$H} NMR (C$_6$D$_6$): $\delta$ 177.88 ($^{H}$ap *C*O), 160.32, 159.96, 136.45, 134.41, 128.83 (br), 128.35, 126.32, 118.28, 109.84, 40.95 (d, $^1J_{PC}$ = 26 Hz, PC), 35.88 (*C*(CH$_3$)$_3$), 34.40 (*C*(CH$_3$)$_3$), 32.24 (C(*C*H$_3$)$_3$), 31.22, 31.10 (C(*C*H$_3$)$_3$), 29.18, 27.54 (d, $J_{PC}$ = 11 Hz), 27.40 (d, $J_{PC}$ = 11 Hz), 26.68. $^{31}$P{$^1$H} NMR (C$_6$D$_6$): $\delta$ −14.44. IR (Nujol mull, cm$^{-1}$): 1589 (s), 1555 (w), 1404 (w), 1379 (s), 1360 (s), 1328 (m), 1307 (m), 1294 (m), 1278 (m), 1258 (s), 1246 (s), 1232 (s), 1193 (m), 1175 (s), 1129 (w), 1105 (w), 1075 (w), 1039 (w), 1025 (m), 1002 (m). UV−vis−NIR (CH$_2$Cl$_2$): $\lambda_{max}$ = 356 nm ($\varepsilon$ = 16 000 L mol$^{-1}$ cm$^{-1}$), 501 nm (11 000), 591 nm (12 000), 910 nm (2200), 1305 nm (1600). Anal. Calcd for C$_{58}$H$_{65}$N$_2$O$_2$OsP: C, 65.63; H, 7.88; N, 2.64. Found: C, 65.51; H, 7.31; N, 2.64.

***cis*-β-($^{H}$ap)$_2$Os(P[OPh]$_3$)$_2$.** To a 20 mL glass vial in the drybox was added 0.3914 g of ($^{H}$ap)$_2$OsO (0.491 mmol), 10 mL of CH$_2$Cl$_2$, 387 μL of triphenylphosphite (1.48 mmol, 3.01 equiv), and a stir bar. The solution changed from dark brown to dark purple upon addition of the phosphite. The vial was capped, and the reaction mixture was stirred for 24 h. The solution was filtered through a fritted glass funnel in the drybox, and the solvent was evaporated from the filtrate on the vacuum line. To the dark residue was added 2 mL of CH$_3$CN. After standing for 3 days under nitrogen, the precipitated solid was isolated by suction filtration and the dark crystals were washed with 2 × 1 mL of CH$_3$CN and dried for 20 min, furnishing 0.2208 g of (32%) *cis*-β-($^{H}$ap)$_2$Os(P(OPh)$_3$)$_2$. $^1$H NMR (400 MHz, toluene-*d*$_8$, 21 °C): $\delta$ 8.20 (br, 1H), 7.49 (br, 1H), 7.39 (s, 1H), 7.22 (br, 2H), 7.11 (t, 8 Hz, 3H), 7.05 (t, 7 Hz, 2H), 6.94 (s, 2H), 6.91 (s, 1H), 6.87 (s, 1H), 6.80−6.58 (m, 30H), 1.60 (s, 9H, $^t$Bu), 1.32 (s, 9H, $^t$Bu), 1.20 (s, 9H, $^t$Bu), 1.08 (s, 9H, $^t$Bu). $^1$H NMR (400 MHz, CD$_2$Cl$_2$, −58 °C): $\delta$ 8.32 (d, 8 Hz, 1H), 7.64 (t, 8 Hz, 1H), 7.37 (t, 8 Hz, 1H), 7.22 (m, 2H), 7.14−6.94 (m, 6H), 6.92−6.65 (m, 22H), 6.41 (d, 7 Hz, 6H), 6.23 (d, 8 Hz, 6H), 1.20 (s, 9H, $^t$Bu), 1.17 (s, 9H, $^t$Bu), 1.13 (s, 9H, $^t$Bu), 0.55 (s, 9H, $^t$Bu). $^{13}$C{$^1$H} NMR (CD$_2$Cl$_2$, −58 °C): $\delta$ 177.66 ($^{H}$ap *C*O), 166.51 ($^{H}$ap *C*O), 160.14, 158.15, 154.28, 152.48 (d, 14 Hz, POC), 151.53 (d, 14 Hz, POC), 150.43, 142.21, 139.39, 137.08, 136.44, 131.05, 129.06, 128.70, 128.37, 128.11, 127.87, 127.74, 126.97, 125.52, 125.05, 124.00, 123.73, 123.05, 120.43, 119.48, 118.35, 112.44, 111.67, 34.60 (*C*(CH$_3$)$_3$), 34.56 (*C*(CH$_3$)$_3$), 34.13 (C(*C*H$_3$)$_3$), 33.96 (*C*(CH$_3$)$_3$), 30.85 (2C, C(*C*H$_3$)$_3$)), 29.12 (C(*C*H$_3$)$_3$), 27.51 (C(*C*H$_3$)$_3$). $^{31}$P{$^1$H} NMR (toluene-*d*$_8$, 21 °C): $\delta$ 57.96 (d, 64 Hz), 50.82 (d, 64 Hz). IR (cm$^{-1}$): 3062 (w), 3041 (w), 3027 (w), 3013 (w), 2999 (w), 2952 (w), 2904 (w), 2866 (w), 1937 (w), 1729 (w), 1590 (m), 1537 (w), 1489 (m), 1455 (w), 1431 (w), 1397 (w), 1382 (w), 1361 (w), 1327 (w), 1304 (w), 1286 (w), 1252 (w), 1226 (m), 1196 (s), 1183 (m), 1160 (m), 1118 (w), 1071 (w), 1024 (m), 1006 (w), 1000 (w), 993 (w), 961 (w), 924 (m), 911 (s), 901 (s), 865 (m), 829 (w), 766 (m), 754 (s), 737 (m), 727 (m), 714 (m), 704 (m), 687 (s), 667 (w), 661 (w). UV−vis (CH$_2$Cl$_2$): $\lambda_{max}$ 362 nm ($\varepsilon$ = 6400 L mol$^{-1}$ cm$^{-1}$), 444 (2400), 522 (3400), 668 (2300), 950 (8400). Anal. Calcd for C$_{76}$H$_{80}$N$_2$O$_8$OsP$_2$: C, 65.13; H, 5.75; N, 2.00. Found: C, 64.85; H, 5.82; N, 1.98.

**Kinetics of Oxygen Atom Transfer.** In the glovebox, a solution of the desired concentration of the oxygen atom acceptor in dichloromethane was prepared. This solution (2.0 mL) was loaded into the large (cuvette) compartment of an angled-reservoir Teflon-sealed (ARTS) cuvette.[27] Into the reservoir of the cuvette was loaded 50−100 μL of an ∼1 mM solution of the oxo complex, and the cuvette was sealed with a Teflon plug and removed from the glovebox. The reaction was initiated by mixing the two compartments, and spectra were recorded on a ThermoFisher Evolution Array or an Agilent 8453 spectrophotometer at 23 °C. For reactions of triarylphosphines, pseudo-first-order rate constants for individual runs were obtained by nonlinear least-squares fitting of the absorbance vs time plots at a single wavelength (typically $\lambda_{max}$ of ($^{R}$ap)$_2$Os(PAr$_3$)) to the expression $A(t) = A_f + (A_0 - A_f)\exp(-k_{obs}t)$ over at least four half-lives. Second-order rate constants were obtained from the slopes of plots of $k_{obs}$ vs PAr$_3$ (Figures S4 and S5). Absorbance vs time data for reactions of tri-*o*-tolylphosphite were fit by nonlinear least squares to the expression characteristic of successive irreversible pseudo-first-order reactions,[28] with $k_{1(obs)}$, $k_{2(obs)}$, and the extinction coefficients of the three species being allowed to vary. In each case, it was found that $k_{1(obs)}$ was greater than $k_{2(obs)}$, as the alternative solution gave rise to unreasonably large extinction coefficients for the equilibrium mixture of monophosphite and *trans*-bis(phosphite) complexes (as judged by comparison to the analogous phosphine complexes). Values of second-order rate constants $k_1$ were determined from the slopes of the linear plots of $k_1$ vs [P(O-*o*-Tol)$_3$] (Figure S6).

**X-ray Crystallography.** Crystals of *trans*-($^{H}$ap)$_2$Os(PPh$_3$)$_2$ were deposited from the reaction mixture of ($^{H}$ap)$_2$OsO with excess PPh$_3$ in benzene, while crystals of *trans*-($^{H}$ap)$_2$Os(CNC$_6$H$_3$-2,6-Me$_2$)$_2$·2 CD$_2$Cl$_2$ were deposited from the reaction mixture of *trans*-($^{H}$ap)$_2$Os(PPh$_3$)$_2$ with xylyl isonitrile in CD$_2$Cl$_2$. Crystals of *cis*-β-($^{H}$ap)$_2$Os(P[OPh]$_3$)$_2$·CH$_3$CN were deposited from the CH$_3$CN solution of the crude material, while crystals of *cis*-β-($^{H}$ap)$_2$Os(P[O-*o*-Tol]$_3$)(NCCH$_3$)·CD$_2$Cl$_2$ were formed when a solution of the reaction mixture between ($^{H}$ap)$_2$OsO and excess P(O-*o*-Tol)$_3$ in CD$_2$Cl$_2$ was layered with acetonitrile. Crystals were coated in hydrocarbon oil before being transferred to the cold N$_2$ stream of the diffractometer ($T$ = 120 K). Data were reduced and corrected for absorption using the SADABS program. After structure solution using Patterson or dual-space methods, non-hydrogen atoms not apparent from the initial solutions were found on difference Fourier maps, and all heavy atoms were refined anisotropically (except for the carbon atom of disordered lattice CD$_2$Cl$_2$ in *cis*-β-($^{H}$ap)$_2$Os(P[O-*o*-Tol]$_3$)(NCCH$_3$)·CD$_2$Cl$_2$, which was refined isotropically).

Hydrogen atoms were found on difference Fourier maps and refined isotropically, except for those in *cis*-β-($^{H}$ap)$_2$Os(P[O-*o*-Tol]$_3$)(NCCH$_3$)·CD$_2$Cl$_2$, which were placed in calculated positions. Calculations used SHELXTL (Bruker AXS),[29] with scattering factors and anomalous dispersion terms taken from the literature.[30] Further details about the structures are given in Table 1.

**Computational Methods.** Computationally, complexes contained "ap" ligands consisting of $^{H}$ap ligands with *tert*-butyl groups and *N*-phenyl substituents replaced with hydrogen atoms. Geometry optimizations were carried out with gas-phase molecules using an SDD basis set for osmium, a 6-31G* basis set for all other atoms, and a B3LYP functional using the *Gaussian 16* suite of programs.[31] Geometries were optimized by minimizing the energies of the compounds, and optimized geometries of stable molecules were confirmed to be minima by the lack of imaginary frequencies in the vibrational analysis or were confirmed to be transition states by the presence of a single imaginary frequency corresponding to a vibration along the reaction coordinate. Calculations on Me$_3$P and Me$_3$PO have been reported previously.[32] Plots of calculated Kohn−Sham orbitals were generated using *Gaussview* (v. 6.0) with an isovalue of 0.04.

## ■ ASSOCIATED CONTENT

### Supporting Information

The Supporting Information is available free of charge at https://pubs.acs.org/doi/10.1021/acs.inorgchem.1c00068.

Additional $^{31}$P NMR spectra, thermal ellipsoid plots, kinetic data, and computational data (PDF)

### Accession Codes

CCDC 2050453−2050456 contain the supplementary crystallographic data for this paper. These data can be obtained free of charge via www.ccdc.cam.ac.uk/data_request/cif, or by emailing data_request@ccdc.cam.ac.uk, or by contacting The Cambridge Crystallographic Data Centre, 12 Union Road, Cambridge CB2 1EZ, UK; fax: +44 1223 336033.


https://dx.doi.org/10.1021/acs.inorgchem.1c00068
Inorg. Chem. 2021, 60, 4004−4014

## AUTHOR INFORMATION


### Corresponding Author

**Seth N. Brown** − *Department of Chemistry and Biochemistry, University of Notre Dame, Notre Dame, Indiana 46556-5670, United States;* orcid.org/0000-0001-8414-2396; Email: Seth.N.Brown.114@nd.edu

### Authors

**Alexander N. Erickson** − *Department of Chemistry and Biochemistry, University of Notre Dame, Notre Dame, Indiana 46556-5670, United States*

**Jacqueline Gianino** − *Department of Chemistry and Biochemistry, University of Notre Dame, Notre Dame, Indiana 46556-5670, United States*

**Sean J. Markovitz** − *Department of Chemistry and Biochemistry, University of Notre Dame, Notre Dame, Indiana 46556-5670, United States*

Complete contact information is available at: https://pubs.acs.org/10.1021/acs.inorgchem.1c00068


### Notes

The authors declare no competing financial interest.

## ACKNOWLEDGMENTS

We thank Dr. Allen G. Oliver for his assistance with the X-ray crystallography. This work was supported by the U.S. National Science Foundation (CHE-1465104). J.G. acknowledges fellowship support from the U.S. Department of Education (GAANN grant P200A1320203-14).

## REFERENCES


(1) (a) Holm, R. H. Metal-Centered Oxygen Atom Transfer Reactions. *Chem. Rev.* **1987**, *87*, 1401−1449. (b) Holm, R. H.; Donahue, J. P. A Thermodynamic Scale for Oxygen Atom Transfer Reactions. *Polyhedron* **1993**, *12*, 571−589.

(2) (a) Pietsch, M. A.; Hall, M. B. Theoretical Studies on Models for the Oxo-Transfer Reaction of Dioxomolybdenum Enzymes. *Inorg. Chem.* **1996**, *35*, 1273−1278. (b) Thomson, L. M.; Hall, M. B. A Theoretical Study of the Primary Oxo Transfer Reaction of a Dioxo Molybdenum(VI) Compound with Imine Thiolate Chelating Ligands: A Molybdenum Oxotransferase Analogue. *J. Am. Chem. Soc.* **2001**, *123*, 3995−4002. (c) Heinze, K.; Marano, G.; Fischer, A. Experimental and theoretical study of a truly functional biomimetic molybdenum oxotransferase analogue system. *J. Inorg. Biochem.* **2008**, *102*, 1199−1211.

(3) Kail, B. W.; Pérez, L. M.; Zarić, S.; Millar, A. J.; Young, C. G.; Hall, M. B.; Basu, P. Mechanistic Investigation of the Oxygen-Atom-Transfer Reactivity of Dioxo-molybdenum(VI) Complexes. *Chem. - Eur. J.* **2006**, *12*, 7501−7509.

(4) Marmion, M. E.; Takeuchi, K. J. Preparation and Characterization of Stable Ruthenium(IV)−Oxo Complexes That Contain Tertiary Phosphine Ligands. *J. Am. Chem. Soc.* **1986**, *108*, 510−511.

(5) Seymore, S. B.; Brown, S. N. Charge Effects on Oxygen Atom Transfer. *Inorg. Chem.* **2000**, *39*, 325−332.

(6) Dixon, J.; Espenson, J. H. Kinetics and Mechanism of Oxygen Atom Abstraction from a Dioxo-Rhenium(VII) Complex. *Inorg. Chem.* **2002**, *41*, 4727−4731.

(7) Jacobi, B. G.; Laitar, D. S.; Pu, L.; Wargocki, M. F.; DiPasquale, A. G.; Fortner, K. C.; Schuck, S. M.; Brown, S. N. Stoichiometric and Catalytic Oxygen Activation by Trimesityliridium(III). *Inorg. Chem.* **2002**, *41*, 4815−4823.

(8) Feng, Y.; Aponte, J.; Houseworth, P. J.; Boyle, P. D.; Ison, E. A. Synthesis of Oxorhenium(V) Complexes with Diamido Amine Ancillary Ligands and Their Role in Oxygen Atom Transfer Catalysis. *Inorg. Chem.* **2009**, *48*, 11058−11066.

(9) Joslin, E. E.; Zaragoza, J. P. T.; Baglia, R. A.; Siegler, M. A.; Goldberg, D. P. The Influence of Peripheral Substituent Modification on $P^{V}$, $Mn^{III}$, and $Mn^{V}(O)$ Corrolazines: X-ray Crystallography, Electrochemical and Spectroscopic Properties, and HAT and OAT Reactivities. *Inorg. Chem.* **2016**, *55*, 8646−8660.

(10) Lee, Y.-M.; Yoo, M.; Yoon, H.; Li, X.-X.; Nam, W.; Fukuzumi, S. Direct oxygen atom transfer *versus* electron transfer mechanisms in the phosphine oxidation by nonheme Mn(IV)-oxo complexes. *Chem. Commun.* **2017**, *53*, 9352−9355.

(11) Topich, J.; Lyon, J. T. Ligand Control of *cis*-Dioxomolybdenum(VI) Redox Chemistry: Kinetic and Activation Parameter Data for Oxygen Atom Transfer. *Inorg. Chem.* **1984**, *23*, 3202−3206.

(12) Dirghangi, B. K.; Menon, M.; Pramanik, A.; Chakravorty, A. A Triad of Variable-Valent Rhenium Aldimine and Amide Systems Interrelated by Successive Oxygen Atom Transfer. *Inorg. Chem.* **1997**, *36*, 1095−1101.

(13) Ison, E. A.; Cessarich, J. E.; Travia, N. E.; Fanwick, P. E.; Abu-Omar, M. M. Synthesis of Cationic Rhenium(VII) Oxo Imido Complexes and Their Tunability Towards Oxygen Atom Transfer. *J. Am. Chem. Soc.* **2007**, *129*, 1167−1178.

(14) Whiteoak, C. J.; Britovsek, G. J. P.; Gibson, V. C.; White, A. J. P. Electronic effects in oxo transfer reactions catalysed by salan molybdenum(VI) *cis*-dioxo complexes. *Dalton Trans.* **2009**, 2337−2344.

(15) Basu, P.; Nemykin, V. N.; Sengar, R. S. Substituent Effect on Oxygen Atom Transfer Reactivity from Oxomolybdenum Centers: Synthesis, Structure, Electrochemistry, and Mechanism. *Inorg. Chem.* **2009**, *48*, 6303−6313.

(16) Smeltz, J. L.; Lilly, C. P.; Boyle, P. D.; Ison, E. A. The Electronic Nature of Terminal Oxo Ligands in Transition-Metal Complexes: Ambiphilic Reactivity of Oxorhenium Species. *J. Am. Chem. Soc.* **2013**, *135*, 9433−9441.

(17) Gianino, J.; Erickson, A. N.; Markovitz, S. J.; Brown, S. N. High-valent osmium iminoxolene complexes. *Dalton Trans.* **2020**, *49*, 8504−8515.

(18) Brown, S. N. Metrical Oxidation States of 2-Amidophenoxide and Catecholate Ligands: Structural Signatures of Metal−Ligand $\pi$ Bonding in Potentially Noninnocent Ligands. *Inorg. Chem.* **2012**, *51*, 1251−1260.

(19) Gianino, J.; Brown, S. N. Highly covalent metal-ligand $\pi$ bonding in chelated bis- and tris(iminoxolene) complexes of osmium and ruthenium. *Dalton Trans.* **2020**, *49*, 7015−7027.

(20) Hübner, R.; Sarkar, B.; Fiedler, J.; Záliš, S.; Kaim, W. Metal(IV) Complexes $[M(L_{N,O,S})_2]^n$ (M = Ru, Os) of a Redox-Active *o*-Amidophenolate Ligand $(L_{N,O,S})^{2-}$ with Coordinating Thioether Appendix. *Eur. J. Inorg. Chem.* **2012**, *2012*, 3569−3576.

(21) Das, D.; Mondal, T. K.; Chowdhury, A. D.; Weisser, F.; Schweinfurth, D.; Sarkar, B.; Mobin, S. M.; Urbanos, F. A.; Jiménez-Aparicio, R.; Lahiri, G. K. Valence and spin situations in isomeric $[(bpy)Ru(Q')_2]^n$ (Q′ = 3,5-di-*tert*-butyl-*N*-aryl-1,2-benzoquinonemonoimine). An experimental and DFT analysis. *Dalton Trans.* **2011**, *40*, 8377−8390.

(22) Das, D.; Agarwala, H.; Chowdhury, A. D.; Patra, T.; Mobin, S. M.; Sarkar, B.; Kaim, W.; Lahiri, G. K. Four-Center Oxidation State Combinations and Near-Infrared Absorption in $[Ru(pap)(Q)_2]^n$ (Q = 3,5-di-*tert*-butyl-*N*-aryl-1,2-benzoquinonemonoimine, pap = 2-Phenylazopyridine). *Chem. - Eur. J.* **2013**, *19*, 7384−7394.

(23) (a) Brown, S. N.; Chu, E. T.; Hull, M. W.; Noll, B. C. Electronic Dissymmetry in Chiral Recognition. *J. Am. Chem. Soc.* **2005**, *127*, 16010−16011. (b) Kongprakaiwoot, N.; Quiroz-Guzman, M.; Oliver, A. G.; Brown, S. N. Gauging electronic dissymmetry in bis-chelates of titanium(IV) using sterically and electronically variable 2,2′-biphenoxides. *Chem. Sci.* **2011**, *2*, 331−336.

(24) Mitra, K. N.; Peng, S.-M.; Goswami, S. Two novel reactions of ruthenated aniline. Structure and bonding in bis-chelated ruthenium complexes of quinone related ligands. *Chem. Commun.* **1998**, 1685−1686.

(25) Scepaniak, J. J.; Margarit, C. G.; Harvey, J. N.; Smith, J. M. Nitrogen Atom Transfer from Iron(IV) Nitrido Complexes: A Dual-Nature Transition State for Atom Transfer. *Inorg. Chem.* **2011**, *50*, 9508−9517.
(26) Erickson, A. N.; Brown, S. N. Molybdenum(VI) tris-(amidophenoxide) complexes. *Dalton Trans.* **2018**, *47*, 15583−15595.
(27) Conner, K. M.; Arostegui, A. C.; Swanson, D. D.; Brown, S. N. When Do Strongly Coupled Diradicals Show Strongly Coupled Reactivity? Thermodynamics and Kinetics of Hydrogen Atom Transfer Reactions of Palladium and Platinum Bis-(iminosemiquinone) Complexes. *Inorg. Chem.* **2018**, *57*, 9696−9707.
(28) Jackson, W. G.; Harrowfield, J. M.; Vowles, P. D. Consecutive, Irreversible First-Order Reactions. Ambiguities and Practical Aspects of Kinetic Analyses. *Int. J. Chem. Kinet.* **1977**, *9*, 535−548.
(29) Sheldrick, G. M. A short history of *SHELX*. *Acta Crystallogr., Sect. A: Found. Crystallogr.* **2008**, *A64*, 112−122.
(30) Wilson, A. J. C., Ed. *International Tables for Crystallography*; Kluwer Academic Publishers: Dordrecht, The Netherlands, 1992; Vol *C*.
(31) Frisch, M. J.; Trucks, G. W.; Schlegel, H. B.; Scuseria, G. E.; Robb, M. A.; Cheeseman, J. R.; Scalmani, G.; Barone, V.; Petersson, G. A.; Nakatsuji, H.; Li, X.; Caricato, M.; Marenich, A. V.; Bloino, J.; Janesko, B. G.; Gomperts, R.; Mennucci, B.; Hratchian, H. P.; Ortiz, J. V.; Izmaylov, A. F.; Sonnenberg, J. L.; Williams-Young, D.; Ding, F.; Lipparini, F.; Egidi, F.; Goings, J.; Peng, B.; Petrone, A.; Henderson, T.; Ranasinghe, D.; Zakrzewski, V. G.; Gao, J.; Rega, N.; Zheng, G.; Liang, W.; Hada, M.; Ehara, M.; Toyota, K.; Fukuda, R.; Hasegawa, J.; Ishida, M.; Nakajima, T.; Honda, Y.; Kitao, O.; Nakai, H.; Vreven, T.; Throssell, K.; Montgomery, Jr., J. A.; Peralta, J. E.; Ogliaro, F.; Bearpark, M. J.; Heyd, J. J.; Brothers, E. N.; Kudin, K. N.; Staroverov, V. N.; Keith, T. A.; Kobayashi, R.; Normand, J.; Raghavachari, K.; Rendell, A. P.; Burant, J. C.; Iyengar, S. S.; Tomasi, J.; Cossi, M.; Millam, J. M.; Klene, M.; Adamo, C.; Cammi, R.; Ochterski, J. W.; Martin, R. L.; Morokuma, K.; Farkas, O.; Foresman, J. B.; Fox, D. J. *Gaussian 16*, Revision C.01; Gaussian, Inc.: Wallingford, CT, 2016.
(32) Hoffman, J. M.; Oliver, A. G.; Brown, S. N. The Metal or the Ligand? The Preferred Locus for Redox Changes in Oxygen Atom Transfer Reactions of Rhenium Amidodiphenoxides. *J. Am. Chem. Soc.* **2017**, *139*, 4521−4531.


https://dx.doi.org/10.1021/acs.inorgchem.1c00068
*Inorg. Chem.* 2021, 60, 4004−4014